Construction and Building Materials 227 (2019) 116616

Contents lists available at ScienceDirect

Construction and Building Materials

journal homepage: www.elsevier.com/locate/conbuildmat

Building materials obtained by recycling coal ash and waste drilling fluid and characterization of engineering properties by means of Artificial Neural Networks

Lucica Anghelescu, Mihai Cruceru, Bogdan Diaconu *

University "Constantin Brâncuși" of Tg-Jiu, Romania

HIGHLIGHTS

- Building material based on ash, waste drilling fluid and clay were developed with the purpose of recycling.
- Compressive strength, density and open pore density of the waste-based materials were assessed.
- An Artificial Neural Network model was developed to model the properties of the waste-based materials.
- Ash and waste drilling fluid are compatible with clay and result in materials with satisfactory properties.
- Influence of components percentage and firing temperature was assessed by means of sensitivity analysis.

ARTICLE INFO

Article history:
Received 3 January 2019
Received in revised form 13 July 2019
Accepted 31 July 2019

Keywords:
Artificial Neural Networks
Ash
Clay
Recycling
Waste drilling fluid

ABSTRACT

Recycling ash from coal combustion deposited in dump sites and waste drilling fluid (WDF) from oil extraction industry for the purpose of partial replacement of clay in construction materials was investigated. Compressive strength, density and pore density were determined experimentally following standard procedures for test specimens manufactured from mixtures of the two waste materials and clay in varying proportions. A neural network model was developed and cross-validated based on experimental data with two purposes: correlating the engineering properties with the material composition and estimating quantitatively the mixture components individual influence on the engineering properties by means of sensitivity analysis (SA). It was found that both ash and WDF are compatible with clay and can partially replace it in construction materials. SA demonstrated that both ash and WDF have the effect of reducing density and compressive strength and increasing pore density.

1. Introduction

1.1. Recycling of coal ash and waste drilling fluid for construction materials

Industrial waste recycling is a matter of increasing concern as the impact on the environment becomes more obvious and irreversible. Ash resulting from coal combustion for power generation is a waste material generated in large amounts throughout the world, causing serious ecological impact on abiotic components. Currently, several directions of use for ash were identified and commercial technologies were developed: concrete production, road base construction, soil amendment, zeolite synthesis, filler in polymers, catalysis, and ceramics [1]. The major components are metallic oxides with varying contents of unburnt organic matter and several oxides, among which the most prevalent are SiO_2, Al_2O_3, Fe_2O_3, CaO, MgO, K_2O [1]. Trace elements such as As, B, Sb, Cd, Co, Cr, Hg, Ni, Pb, Cs, etc. can be identified [2]. Ash resulting from coal combustion consists of large particle size (bottom ash, 5–20%) and fine fly ash (80–95%). Recycling applications exist mainly for fly ash (FA), while in the case of bottom ash, non-homogenous character and presence of organic matter limit the range of applicability. Although many different uses and recycling directions exist for ash, only roughly 42% of the current production is utilized [3]. For existing ash ponds and ash dump sites a very limited number of solutions exist and they are case-specific.

Construction materials industry has developed technologies and processes to integrate ash (mainly FA, with low content of

* Corresponding author at: University "Constantin Brâncuși" of Tg-Jiu, Eroilor 30, Tg-Jiu, Romania.
E-mail address: diaconu@utgjiu.ro (B. Diaconu).

https://doi.org/10.1016/j.conbuildmat.2019.07.342
0950-0618/

unburned carbon) into finite products such as concrete and various building elements. A comprehensive review of FA applications in construction materials industry can be found in [4]. The traditional use of FA is in concrete mix in amounts ranging from 15% to 30% from the cementitious binder [4]. Ash used in mixtures with Portland cement contributes to the properties of the hardened concrete through hydraulic or pozzolanic activity, or both [5].

Leiva et al [3] conducted and experimental study, using FA in mixture with clay for manufacturing of fired bricks. Six test specimens were manufactured including clay-only and FA-only specimens, which were fired at 800, 900 and 1000 °C. It was found that addition of FA influences to a significant level the physical properties of the test specimens (compressive strength, water absorption and density). It has been also determined that the properties of the finite product depend on the ash Loss on Ignition (LOI) value to an important extent.

Abbas et al [6] fabricated experimental brick specimens using six FA – clay dosages (0–100, 5–95, 10–90, 15–85, 20–80 and 25–85). The wet bricks were allowed to dry for 4–5 days in open air and then fired in the kiln for three days at approximately 800 °C. Burnt bricks were taken out of the kiln after cooling down for 20 days. Addition of FA resulted in a significant reduction of the compressive strength (from approximately 19 MPa at 5% FA to 7.5 MPa at 25% FA). Water absorption increased significantly with addition of FA reaching values two times higher than those corresponding to clay-only bricks. Lingling et al [7] manufactured clay-FA bricks from a mixture clay – FA with a low value of the LOI (2.82%). The firing temperature was 1000, 1050 and 1100 °C, in the range of the ash sintering temperature. The influence of the FA particle size was investigated. It was found that the compressive strength of the finite product is influenced in the sense of increasing as the mean particle size decreases. This trend was explained by the sintering kinetics theory, (the sintering force is inversely proportional to the particle radius [8]).

Waste drilling fluid (WDF) from oil industry is another material with less recycling options than ash. Drilling fluid consists usually of a mixture of water, bentonite clay and other chemicals and serves several purposes (such as carrying the cuttings form the bottom of the well to the surface, cooling the drilling bit, pressure control, etc.). Drilling cuttings carried to the surface by the drilling fluid constitute the waste part and consist of a mix of various rock types particles.

WDF from oil extraction industry is currently disposed by direct landfill, thermal treatment, solid-liquid separation, stabilization/solidification and bioremediation [9,10]. A comprehensive chemical analysis of the WDF is given in [10]. The physical and chemical properties of the drilling wastes determine its hazardous characteristics and environmental impact potential. WDF undergoes complex treatment and handling processes which increase the operation cost of the oil drilling rigs [11]. Conventional disposal practices are onsite burial, land farming, thermal treatment, slurry injection and bioremediation [12].

Recycling of WDF for producing lightweight aggregate has been investigated by Ayati et al [13]. Drill cuttings produced from the North Sea oil field were dried, ball milled, formed into pellets and fired at temperatures between 1160 and 1190 °C. Sintering at 1180 °C produced lightweight aggregate with particle density 1.29 g/cm^3, water absorption 3.6% and compressive strength 4.4 MPa.

Mostavi et al [14] assessed the feasibility of using drill cuttings in concrete as a partial replacement of cement. Drill cuttings resulted in reduction of the compressive strength. It was found that the drop in compressive strength can be compensated by FA or silica fume addition.

1.2. Modeling properties of construction materials by means of Machine Learning Algorithms (MLA)

Key properties of construction materials manufactured from raw materials are influenced in complex ways and not fully understood by the mixture components proportions and fabrication process flow. In addition to statistical methods that have been used traditionally to quantify and control properties required by specific standards, MLA based methods have been increasingly employed in modeling properties of construction materials. Among MLAs, Artificial Neural Networks are particularly interesting as they are capable of developing accurate models from empirical data without knowledge of physical mechanisms [15], which most of the times cannot be described analytically, given the large number of factors influencing the characteristics of the finite product.

Naderpour et al [16] presented a literature review of MLA techniques employed to model properties of HPCs, concrete containing blast furnace slag and FA, concrete containing Haydite LWA and PLC and the input variables for each model. The sample size and the performance of the model (quantified through the value of the correlation coefficient between measured and predicted values sets) were also listed. Compressive strength of the finite product was the output of the models.

Young et al [15] compared statistical and MLA techniques employed to predict compressive strength of concrete as a function of its mixture proportions. A dataset with over 10,000 measured compressive strength values was used. It was found that the models can predict the compressive strength with an average relative error of less than 10%.

Deng et al [17] modeled the compressive strength of concrete based on recycled coarse aggregate by means of three prediction models, Back Propagation Neural Network (BPNN), Support Vector Machine (SVM) and Convoluted Neural Network (CNN). It was found that the best performance was achieved in the case of CNN with a relative error of 3.65%. As mechanical properties are critical performance criteria for construction materials most studies based on MLAs focus on modeling such properties.

Getahun et al [18] modeled the strength of a concrete incorporating various construction debris and agricultural waste. A fifteen-input, one fifteen-neuron hidden layer and two outputs (compressive strength and tensile splitting strength) model was used. Model performance for three types of activation functions was studied. A data set consisting of 66 entries were used. The model performance was assessed in terms of absolute and relative error between the measured values and predicted values. The mean relative error reported was 2.90% and the correlation coefficient determined for the whole set was 0.9811.

Naderpour et al [16] developed a BPNN model to predict compressive strength of concrete fabricated based on recycled aggregates. The objective of the study was to assess the feasibility of substituting natural aggregate with recycled aggregate. A data set consisting of 139 samples was used to train the network. A 6-18-1 MLP topology was chosen resulting in a correlation coefficient value of 0.89 and regression model parameters (slope and intercept) 0.82 and 0.084.

Alexandridis et al [19] presented a non-destructive method for predicting the compressive strength of cement-based materials employing a radial basis function network. A relative error between measured and predicted values of approximately 1% and a Pearson correlation coefficient of 0.7 or higher were reported.

Šipoš et al [20] used an ANN model to simulate material properties of concrete with crushed brick and roof tile aggregate. It was found that the eight-input model predicted the compressive strength of the recycled brick aggregate concrete with a maximum relative error of 14%. The ANN model allowed quantifying the

effect of coarse/fine aggregate application on the value of the compressive strength.

Trocoli et al [21] used an ANN to predict the compressive strength of concrete using construction and demolition waste employing experimental data from literature. A number of 1178 samples were used for an ANN with 17 inputs and one output only – compressive strength. The inputs of the model were selected based on Principal Component Analysis. The correlation coefficient for training and for testing was 0.928 and 0.971 respectively and the. Relative errors between 20 and 50% occurred in 4.6% of points and larger than 80% in 0.4% of points.

Duan et al [22] developed an ANN model to predict the compressive strength of recycled aggregate. A 14 (input) – 16 (hidden) – 1 (output) neurons topology was used. The data set consisted of 168 entries from 17 literature sources. The relative error between measured and predicted values of the compressive strength ranged from 0.2% to 16.3% with an average of 5.85%.

A comprehensive discussion on Artificial Neural Networks can be found in classic textbooks such as [23,24].

2. Experimental procedure

The study consisted of two main parts: (I) manufacturing test specimens based on various proportions of clay, ash and WDF followed by firing at different temperatures and determining experimentally the main physical properties: compressive strength, apparent density and open pore density (porosity) and (II) developing an Artificial Neural Network based on the experimental data obtained in the first part to (i) predict physical properties of the final products and (ii) examine the individual influence of input variables on the physical properties of the final product.

Raw ash and WDF were minimally pre-processed and prepared as follows:

- Raw ash collected from a dump site was sieved and only fraction less than 4 mm was used in the study.
- Test specimens manufactured from mixtures with more than 60% WDF required drying of WDF prior to prepare the mixture as it was observed that the high humidity of the raw WDF resulted in a high fluidity mix, unsuitable for pressing and extrusion.

2.1. Materials

The objective of the study was to assess the opportunity of recycling ash and WDF as a (partial) substitute for clay, keeping the expenditures for pre-processing of ash and WDF to a minimum. The study was focused on ash accumulated over time in dump sites. This kind of ash is different from FA – which can be considered high-grade ash – due to the following:

- Large standard deviation of the particle size distribution (PSD)
- Large content of organic matter due to the presence of bottom ash (which is known to contain the most part of incompletely burned coal)
- Exposure to environmental factors in the dump site over time can alter significantly the properties of ash, including the organic matter content.

2.1.1. Ash from coal combustion

The ash samples used in this study were collected from the dump site Valea Ceplea (Romania) covering a surface area of 52.64 ha and a volume of approximately 13 mil m^3. Chemical analysis indicated that approximately 70% represents aluminum oxide and silica, as shown in Table 1, where oxide composition is presented for four arbitrary samples. Due to the large dimensions it was considered important to sample various depths of the dump site (5 m, 10 m, 15 m and 20 m). It was found that the depth of the sample influences especially SiO_2 content and LOI, as shown in Table 1. All ash samples can be categorized in the oxide class $SiO_2 – Al_2O_3 – Fe_2O_3 – CaO$, being similar to feldspars and clays. Given the large size of the dump site, samples were collected from several zones. The PSD size was determined by sieve analysis. The results are presented in Table 2.

A key issue regarding ash is the content of organic matter, which is quantitatively described by LOI or fixed carbon values. The presence of organic matter influences negatively the potential of ash to be used in mixtures for fabrication of construction materials. However, it was considered interesting to assess the feasibility of using waste materials in raw state, without any pre-processing stage, such as removal of organic matter, etc.

2.1.2. Waste drilling fluid (WDF)

WDF evacuated from oil drilling rigs (containing rock cuttings and detritus extracted from Pontian and Dacian strata situated at depths ranging from 600 to 1400 m) from oil drilling site Oprisenesti (Romania) was used in this study. WDF has a composition similar to that of calcium-silica clays: 50–55% SiO_2, 8–12% Al_2O_3, 3–5% Fe_2O_3, 7–10% CaO, 2–3% MgO, 3.5–5.5% $Na_2O + K_2O$ and LOI 13–15% [40]. WDF appears like a dark grey, high-viscosity paste (Fig. 1). Due to the water content it has reduced plasticity (does not retain the shape obtained by mechanical deformations).

2.1.3. Clay

Clay was used as plastifying agent for all mixtures considered in this study. The clay used in mixtures resulted from stripping operations at the lignite open pit mine Roşia de Jiu (Romania). The oxide chemical composition is presented in Table 3. Pre-processing consisted of drying at room temperature followed by grinding in a laboratory vibrating cup mill for three minutes. The grinded clay was integrally used in mixtures with no prior particle size separation.

An important point regarding clay is the PSD presented in Table 4. A significant difference exists between PSD for clay (Table 4) and ash (Table 2) with 88% consisting of particles less than 0.06 mm (clay) and roughly 20% consisting of particles larger than 0.2 mm (ash). Such difference causes significant variations in the standard deviation of the PSD for the mixtures prepared, which influence the dynamics of the sintering process.

2.2. Methods

Mixtures consisting of coal ash (*A*), waste drilling fluid (*WDF*) and clay (*C*) as plastifying agent were prepared by dosing each component in terms of weight percentage. The mixtures variants and range of component dosage are presented in Table 5. A total number of 69 dosing variants were prepared.

Components of the mixture added up to approximately 6 kg for each dosing variant in order to obtain enough raw material to manufacture a minimum of 20 test specimens. The number of the test specimens was selected preparing two identical (dosage and firing temperature) sets of samples and increasing successively the number of test specimens until the differences of mean values of the two samples for compressive strength, density and pore density was less than 2%.

Mixing was carried out adding gradually water in order to achieve the desired plasticity and to check permanently if aggregation tends to occur. Water addition stopped when the first signs of aggregation were noticed. Aggregation is caused mainly by clay, which has the natural tendency to form lumps. The mixing continued until separation of the mixture phases was no longer visible. The mixture was conserved for 24 h in airtight polyethylene bags in order to ensure uniform distribution of water in the material. The test specimens were manufactured by placing approximately 200 g of material into a cylindrically-shaped mould, pressing the material by means of a mechanical forming press with a maximum force of approximately 10 tons, followed by extrusion to extract the test specimen from the mould. The amount of raw mixture placed into the mould was adjusted by trial and error in order to obtain uniformity in test specimens height (approximately 50 mm). The mould used was a steel cylinder with inner diameter 50.0 mm. The phases of the test specimen manufacturing are presented in Fig. 2. Test specimens were conditioned at room temperature for 24 h and then were subject to moisture removal by drying at 110 °C for 10 h. The appearance of several test specimens after drying is shown in Fig. 3.

The firing of the test specimens was carried out in a resistance oven starting with a heating rate of 3 °C/min, followed by a plateau phase at the maximum temperature for three hours ending with free cooling in the oven. The final appearance of the test specimens after firing is shown in Fig. 4. The firing temperature range was selected by means of trial and error, observing that at temperature values less than 950 °C and more than 1050 °C some specimens (especially those with high ash

Table 1
Oxide composition of ash compared to a standard clay for different depths [40].

	Sample no	SiO_2	TiO_2	Al_2O_3	Fe_2O_3	MgO	CaO	MnO	Na_2O	K_2O	P_2O_5	SO_3	LOI
Ash	1 (5 m)	49.7	0.77	20.95	8.96	2.48	9.25	0.08	0.21	1.55	0.2	0.59	12.06
	2 (10 m)	40.8	0.67	15.7	8.4	2.36	13.75	0.08	0.19	1.35	0.21	4.6	11.69
	3 (15 m)	45.24	0.76	19.15	8.65	2.35	9.45	0.07	0.2	1.44	0.24	1.52	10.73
	4 (20 m)	46.8	0.68	19.4	8.9	2.42	9.35	0.08	0.25	1.42	0.24	1.38	8.88
Clay [33]		47.7	1.7	21.65	7.1	0.8	1.9	0.16	–	0.8	0.11	–	–

Table 2
Grain size distribution of ash sampled from five zones of the dump site [40].

Sample	Humidity	Grain size distribution Retained (%w) on the sieve with gauge (mm)									Density g/cm^3	
Dump site zone	%	4	3	2	1	0.5	0.2	0.09	0.06	<0.06	Bulk	Tapped
1	29.46	2.55	1.23	2.10	5.11	7.75	18.66	25.55	9.13	27.91	0.77	0.97
2	29.53	3.24	1.35	2.25	5.57	8.10	19.22	25.86	8.50	25.92	0.79	0.97
3	25.04	3.37	1.86	2.93	5.96	7.95	19.07	25.53	7.99	25.33	0.76	0.96
4	28.68	5.43	1.80	2.44	5.81	7.80	18.56	25.36	8.03	24.76	0.79	0.98
5	28.72	3.17	1.68	2.28	5.58	8.12	19.41	26.70	8.62	24.44	0.76	0.96

Fig. 1. Waste drilling fluid, raw state.

content) exhibit structural issues (visible cracks, brittleness, and especially friability). As a result, the firing temperature interval was limited to 970–1030 °C. Preliminary tests showed that temperature influences the engineering properties of the samples to a lesser extent than components dosage. It was established that a number of firing temperature values higher than three is not justified. The firing temperature values were 970 °C, 1000 °C and 1030 °C.

Determination of the compressive strength of the test specimens was carried out according to SR EN 993-5 [25] (Fig. 5). The equipment used was an EN 12390-3, 12390-4, BS 1881, ASTM C39 compliant automatic compression testing machine. The test machine was programmed to apply a force with a gradient of 0.2 MPa/s until the break of the test specimen occurred. For each determination 12 test specimens were used. Outliers – defined as more than 1.5 IQR (Inter-Quartile Range) away from the nearest quartile [26] were eliminated and the final value recorded was considered the mean of the remaining values.

The provisions of the standard SR EN 993-1 [27] were employed for determining the apparent density and open pore density (porosity) of the test specimens. The apparent density was determined by measuring the physical dimensions with a precision of 0.1 mm and weighing the test specimens with a precision of 0.01 g. In order to determine the apparent density and open pore density the test specimens were immersed in water and boiled for 2.5 h in to ensure filling of the porous structure, then weighed in air and hydrostatically.

The oxide composition for several dosages for test specimens fired at 1000 °C is presented in Table 6. It can be noticed that the products follow a quaternary oxide system similar to that of the waste materials considered, $SiO_2 – Al_2O_3 – Fe_2O_3 – CaO$.

3. Results and discussion

3.1. Development of the ANN model

A feed-forward, multi-layer perceptron ANN model has been employed to process the engineering properties of the materials obtained, which are expected to be influenced by the varying parameters: clay, ash, and WDF percentage values and firing temperature. A standard ANN architecture with one input layer, one hidden layer and one output layer (MLP) has been selected with logistic sigmoid as activation function. The predictive model for compressive strength (CS), apparent density (D) and open pore density (PD) of the waste materials - based construction material has been developed considering as input parameters the mixture components percentages, clay (C) [%], ash (A) [%] and waste drilling fluid (WDF) [%] and firing temperature (T) [°C]. A three-layer feed-forward neural network architecture $N : I \rightarrow O$, where I is the input set (four dimensions) and O is the output set (three dimensions) was chosen to model the physical properties of the materials. The training algorithm was chosen Bayesian Regularization [28]. Although more slowly converging, this algorithm was chosen due to its efficiency in cases of small data sets, complex relationships between inputs and outputs and noisy data. Details on implementation of Bayesian Regularization ANN training algorithm can be found in [29]. The input set was divided in 70% training, 15% validation and 15% testing. The performance criteria used in the training algorithm was selected Mean Squared Error.

Table 4
Clay particle size distribution.

Humidity (%)	Retained (%w) on the sieve (mm)		
8.65	0.09	0.06	<0.06
	2.6	9.4	88.0

The data set resulting from experiments consisting of 207 entries (69 dosing variants × 3 values of the firing temperature) was divided selecting 60% (DS_1, 123 samples) for NN model training and the rest for validation and investigation of other effects (DS_2, 84 samples). The validation data set was designed considering the following:

- Mixture components dosage were maintained within corresponding maximum and minimum limits of the training set;
- Since it was observed from preliminary tests that temperature influence is less significant than components dosage (especially on density), the same firing temperature values as in the training set were used (970 °C, 1000 °C and 1030 °C). For firing temperature differences between identical samples (in terms of components dosage) less than 30 °C it was not certain whether density differences were caused by temperature or by inherent measurement errors.

Commercial package Matlab 2015 with Neural Network Toolbox was used to develop the model and to produce the scripts and functions that were further employed in simulations.

Table 3
Clay oxide composition [40]

Oxide compounds (%w)										LOI
SiO_2	TiO_2	Al_2O_3	Fe_2O_3	MnO	MgO	CaO	Na_2O	K_2O	P_2O_5	
65.80	0.68	15.97	5.40	0.11	1.64	0.85	1.86	2.37	0.12	5.35

Table 5
Mixture variants and dosage ranges.

Dosage range per component	Components					
	C-A	C-WDF	WDF-A	C-WDF-A	C	WDF
C	98…45	50–80	0	60…20	100	0
A	2…55	0	30–50	60…20	0	0
WDF	0	20–50	50–70	20…60	0	100

Fig. 2. Manufacturing the test specimen – pressing and extrusion.

3.1.1. Selection of topology and output of the model

In order to select the ANN topology, three values of the learning rate (0.2, 0.5 and 0.7) were considered and the number of neurons in the hidden layer was varied from 5 to 35. For each value of the learning rate, the performance of the model was assessed by determining the following parameters:

- Pearson correlation coefficient R:

$$R = \frac{\sum_{i=1}^{N}(x_i-\bar{x})(y_i-\bar{y})}{\sqrt{\sum_{i=1}^{N}(x_i-\bar{x})^2}\sqrt{\sum_{i=1}^{N}(y_i-\bar{y})^2}} \quad (1)$$

- Root mean square error $RMSE_i$ (Eq. (8)) between y_{ij} and y_{ij}^p $(i = 1\cdots N_O, j = 1\cdots N)$:

$$RMSE = \sqrt{\frac{1}{N}\sum_{i=1}^{N}\left(y_{measured}-y_{predicted}\right)^2} \quad (2)$$

- Mean of relative errors ε_i:

$$\varepsilon_i = \frac{1}{N}\sum_{j=1}^{N}\frac{\left|y_{ij}-y_{ij}^p\right|}{y_{ij}} \times 100 (i = 1\cdots N_O, j = 1\cdots N \quad (3)$$

- Slope (a_i) and intercept (b_i) of the LSE regression model between $\left(y_{ij}, y_{ij}^p\right)$

For each value of the learning rate the corresponding N_h was selected based on maximum $\sum_{i=1}^{N_O}\left(R^2\right)$ criterion. Selecting the sum of correlation coefficients for *CS*, *D* and *PD* as optimization criterion ensures simultaneous optimization for all three outputs. Linear regression model parameters for the three values of the learning rate and for the N_h that maximized the sum of correlation coefficients are presented in Fig. 6 for the training data set DS_1. The values of N_h for the three values of the learning rate considered (0.2, 0.5 and 0.7) for which the sum of correlation coefficients was maximized were 24, 25 and 31 respectively. The optimum value of the learning rate was selected based on sum of correlation coefficients and relative error for all outputs. The optimization parameters are presented in Table 7. From Table 7 it can be observed that the best performance is achieved for network parameters $LR = 0.7$ and $N_h = 31$. Regression analysis performed on the outputs of the network ($LR = 0.7$, $N_h = 31$) are summarized in Table 8, correlation coefficients, RMSE and mean of relative errors are presented in Fig. 6. The outputs of the ANN model with $LR = 0.7$ and $N_h = 31$ are presented in Fig. 7.

3.1.2. Error analysis

The ANN model fails to predict the compressive strength within 10% relative error for 3 samples, apparent density within 2% for 5 samples and pore density within 3% for 3 samples, as shown in Fig. 8. The model overpredicted the compressive strength with an average of 0.009 MPa, overpredicted the apparent density by 2.5E-4 kg/m^3 and underpredicted pore density by 0.014%. Regression analysis between measured values and the corresponding residuals resulted in Pearson coefficient values that suggest that no significant correlation exists (*CS*: $R^2 = 0.0389$ *D*: $R^2 = -0.056$, *PD*: $R^2 = 0.093$). Although the performance of the model can be considered satisfactory it is not only the average error that is important. The main error parameters are summarized in Table 9. The estimation precision is comparable with other results reported [15,22].

3.2. Sensitivity analysis

A large number of methods for quantifying the importance of variable in terms of output influence exist [30]. Olden et al [31] reviewed and compared Connection Weight Approach with Garson's algorithm. It was found that Garson's algorithm [32,33] although the most commonly used in statistical ecology studies [31], performed the worst in ranking the inputs based on the influence on outputs. Garson's algorithm determines the influence of input variable i on output variable o by the equation:

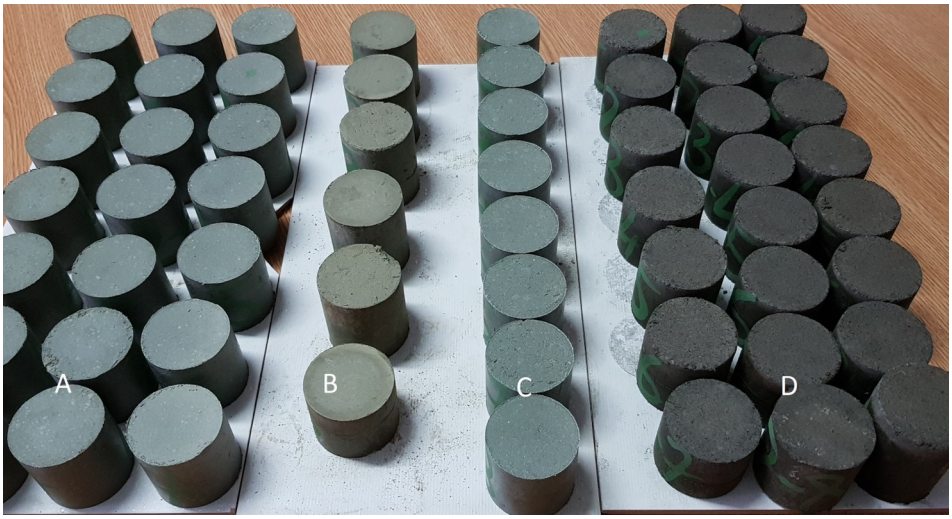

Fig. 3. Test specimens after drying: A – clay + ash, B – WDF, C – clay, D – WDF + ash.

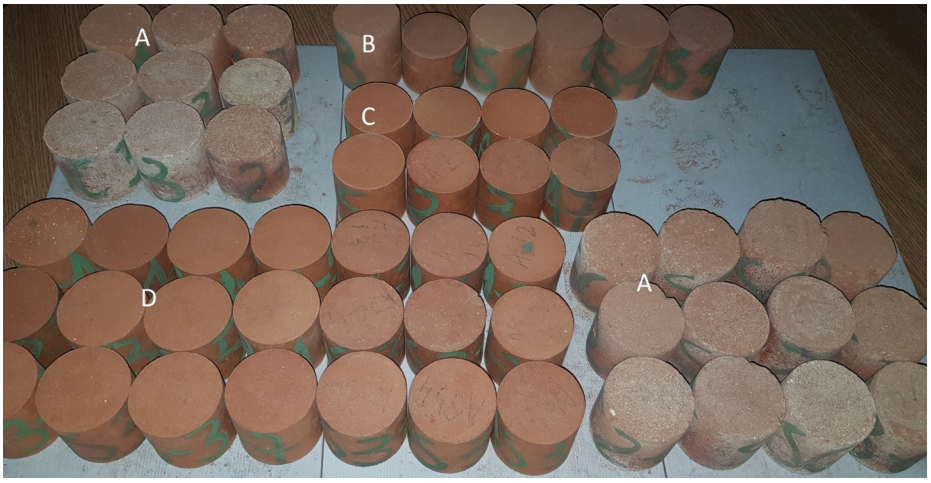

Fig. 4. Test specimens after firing: A – Ash + WDF, B – WDF, C – Clay, D – Clay + WDF.

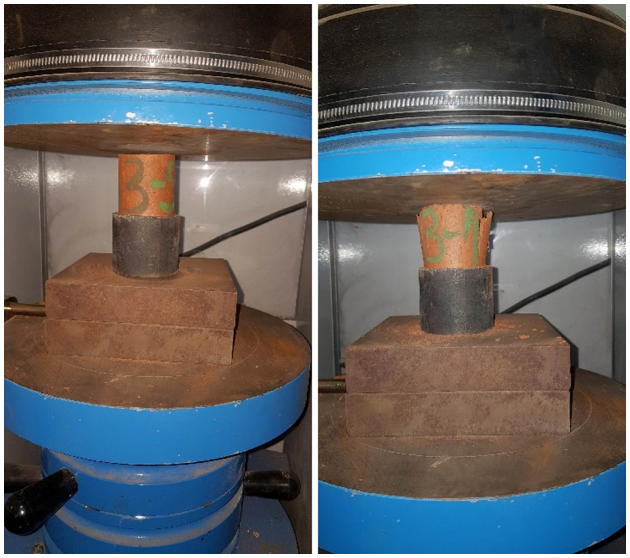

Fig. 5. Determination of the compressive strength.

$$R_{oi} = \frac{\sum_{j=1}^{N_h}\left(\frac{\left|w_{ji}^{IH}\right|}{\sum_{l=1}^{N_i}\left|w_{jl}^{IH}\right|}\cdot\left|w_{oj}^{HO}\right|\right)}{\sum_{k=1}^{N_i}\left(\sum_{l=1}^{N_h}\left|\frac{w_{ji}^{IH}}{\sum_{l=1}^{N_i}\left|w_{jl}^{IH}\right|}\cdot w_{oj}^{HO}\right|\right)} \tag{4}$$

Due to the fact that Garson's algorithm uses absolute values of the weights it cannot indicate the direction of influence (positive or negative) and it may also underestimate/overestimate some influences [31,34].

Another sensitivity metric for an ANN model is Spearman rank-order coefficient (SPEA) [30]. SPEA will be used in this study to verify the hypothesis that a functional dependence (not necessarily linear like in the case of Pearson correlation coefficient) exists between outputs and inputs of the ANN model and to detect the presence of random components in the outputs. The following sets will be used to determine SPEA values:

$$\left[\tilde{x}_{ij}\right]_{N_G},\ i = 1\ldots N_I,\ j = 1\ldots N_S$$

$$\left[\tilde{y}_k^{(x_{ij})}\right]_{N_G},\ k = 1\ldots N_O \tag{5}$$

Table 6
Oxide composition determined for finite products for several mixture variants [40].

Dosage	Oxide composition (% w)												
	SiO_2	Al_2O_3	Fe_2O_3	TiO_2	Na_2O	K_2O	CaO	MgO	MnO	P_2O_5	LOI	$S_{pyritic}$	SO_3
C-90% A-10%	61.90	20.61	6.48	0.86	1.40	3.23	2.71	1.91	0.12	0.01	0.36	0.09	0.15
C-70% A-30%	59.21	21.37	6.77	0.86	1.26	2.98	4.28	2.07	0.10	0.01	0.65	0.19	0.41
C-40% A-60%	54.60	22.71	7.80	0.86	0.98	2.61	6.71	2.39	0.09	0.02	0.80	0.25	0.65
C-20% A-20% D-60%	62.90	18.32	6.18	1.03	1.68	2.85	4.14	1.91	0.14	0.02	0.44	0.06	0.09

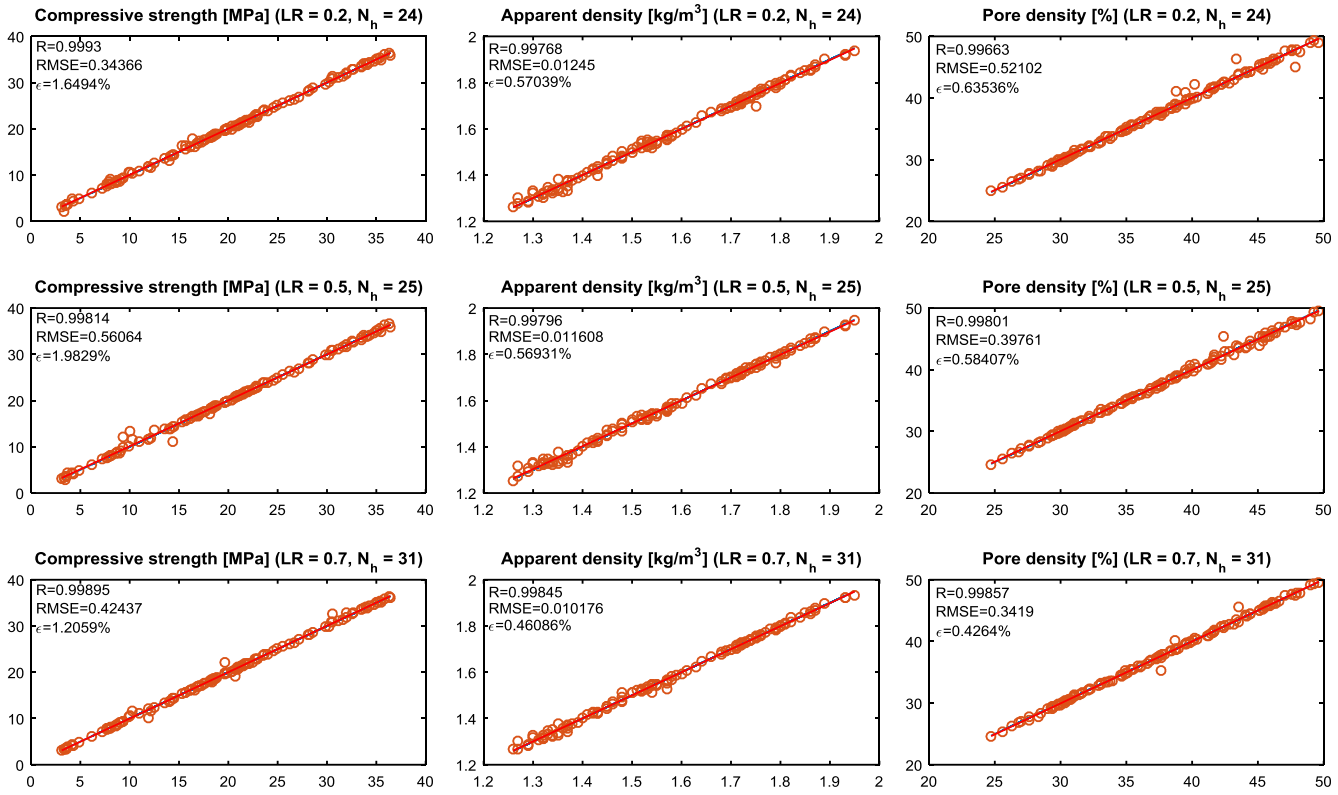

Fig. 6. Linear fit of measured – predicted set of values for CS, D and PD.

Table 7
Sum of correlation coefficients and relative error for the three learning rate values.

Optimization parameter	$LR = 0.2$, $N_h = 24$	$LR = 0.5$, $N_h = 25$	$LR = 0.7$, $N_h = 31$
$\sum_{i=1}^{N_O} \left(R^2\right)_i$	2.9936	2.9941	2.9960
$\sum_{i=1}^{N_O} \varepsilon_i$	3.5111	3.8584	2.5744

Spearman rank-order coefficients for compressive strength, density and pore density were plotted in Fig. 9 for all samples considered in the test set X_S. The variable altered was clay percentage (to which Gaussian noise was applied with mean value x_{1j} with $j = 1 \cdots N_S$ and four values of the standard deviation 0.5, 1.5, 2.5 and 3.5) and ash percentage was corrected to have $C + A = 100 - D$. For low values of the standard deviation of the input variable (clay %) most values of SPEA are close to 1 or −1 indicating a significant functional dependence. SPEA values tend to disperse in the interval $[-0.9, 0.9]$ as the standard deviation increases, as shown in Table 10 A.

Spearman rank-order coefficient can predict the existence of a functional dependence in case of monotonically functions only (positive values for monotonically increasing and negative for monotonically decreasing functions). In case of existence of a

Table 8
Parameters of the linear regression model (measured – predicted values).

Output	CS		D		PD	
Parameter	Slope	Intercept	Slope	Intercept	Slope	Intercept
Value	1.0018	−0.0258	0.9969	0.00494	1.005	−0.2026
Std err	0.00418	0.09035	0.0050	0.00802	0.0049	0.186
t-Stat	240	−0.2858	197	0.6166	205	−1.09
p value	0	0.7755	0	0.538	0	0.278
LCL	0.994	−0.205	0.987	−0.011	0.995	−0.571
UCL	1.01	0.153	1.007	0.021	1.015	0.166

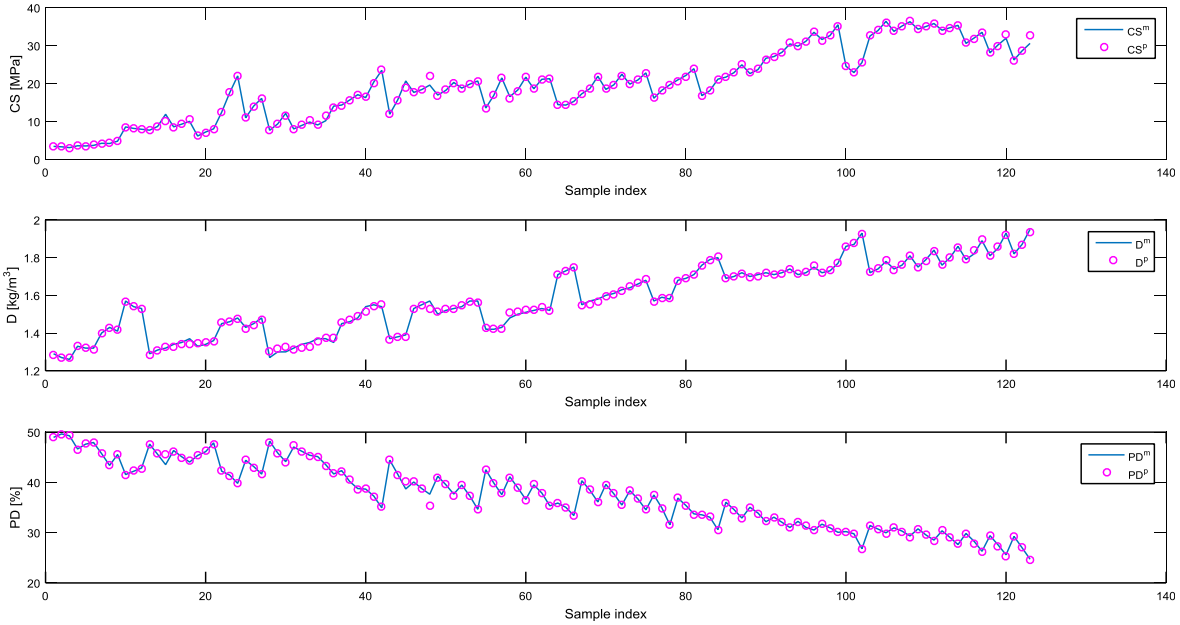

Fig. 7. ANN model predicted (y_i^p) and measured (y_i^m) values.

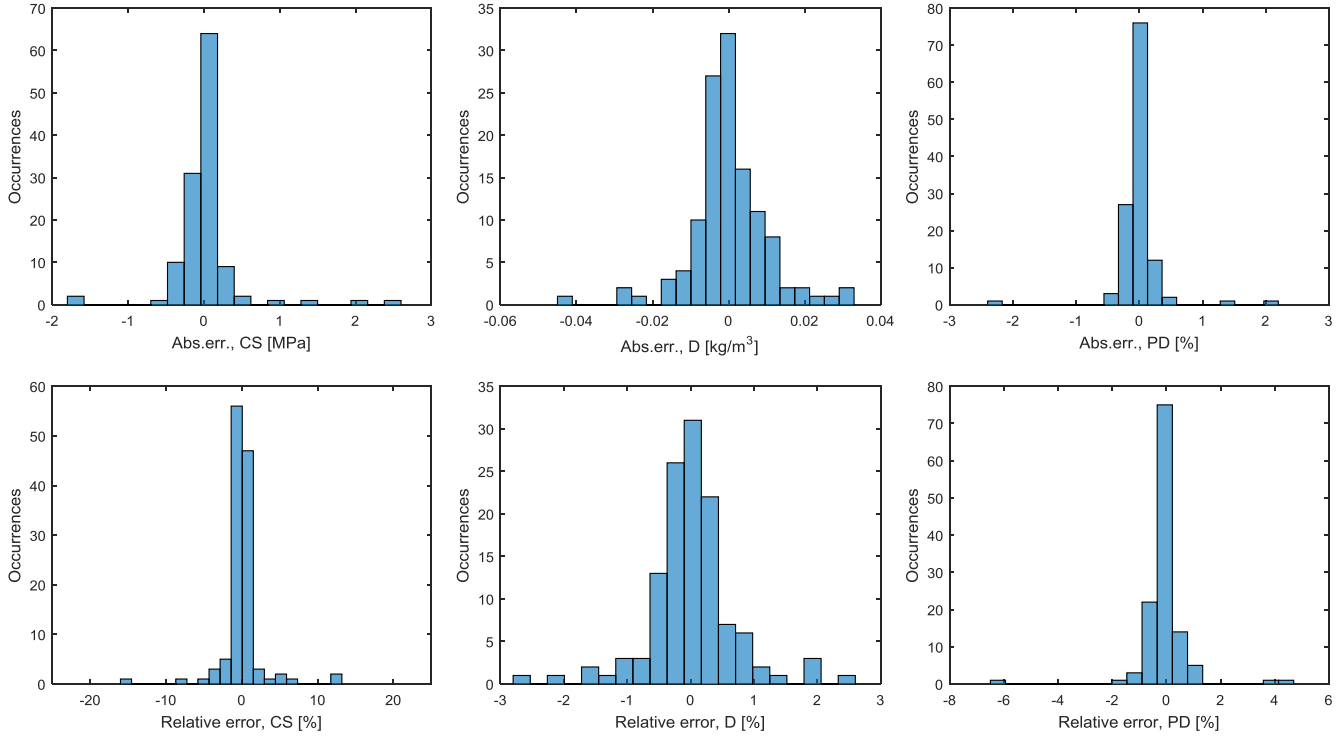

Fig. 8. Absolute and relative errors predicted – measured values.

non-monotonic functional dependence (e.g. a local extreme is present) SPEA will have values (absolute) closer to zero, pointing to the conclusion that there is no tendency in output caused by variations of the input variable and the model produces erratic results. The output of the model can be analyzed by plotting the output corresponding to the set $\left[\tilde{x}_{1j}\right]_{N_G}$, $i = 1\ (C\ \%)$, $j = 1 \ldots N_S$. In Fig. 10 the compressive strength was plotted against clay percentage for the case where clay percentage set was generated from Gaussian noise centered at x_{1j} (with j values such as clay % varied from 40 to 100%) and standard deviation 0.5. Ash percentage was varied correspondingly to maintain $C + A = 100\%$ (only points with WDF =0% were included in Fig. 10). Markers (cross) correspond to CS measured values (x_{1j}, y_{1j}) while lines of the same color correspond to outputs of the ANN for the input sets $\left[\tilde{x}_{1j}\right]_{N_G}$, which is $\left[\tilde{y}_{1j}\right]_{N_G}$. For each value of the clay % three distinct point exist corresponding to three values of the firing temperature. Left and right limits of the sets $\left[\tilde{x}_{1j}\right]_{N_G}$ extend as far as the chosen standard devi-

Table 9
Absolute and relative errors of the ANN predicted values.

	Mean		Max	
	Abs	Rel	Abs	Rel
CS	0.190	1.205	2.45	15.0
D	0.007	0.460	0.04	2.74
PD	0.160	0.426	2.33	6.19

ation value allows. Depending on the distance from x_{1j} to x_{1j+1} points, sets $\left[\tilde{x}_{1j}\right]_{N_G}$ and $\left[\tilde{x}_{1j+1}\right]_{N_G}$ can overlap or gaps can exist, as shown in Fig. 10. While no apparent random behavior can be observed in $\left[\tilde{y}_{1j}\right]_{N_G}$ sets, a local extreme point exists located at abscissa values between 80 and 90%. This explains the apparent failure of SPEA to predict a strong functional dependence between $\left[\tilde{y}_{1j}\right]_{N_G}$ and $\left[\tilde{x}_{1j}\right]_{N_G}$ for some points, especially as the standard deviation in input increases.

The imbalance between SPEA values higher than 0.9 and lower than −0.9 is an indication of the dependence type (increasing or decreasing) between varying input variables (clay and ash %) and outputs. Based on this observation it is useful to examine the influence of the other input variables. Distribution of the SPEA values in the interval $[-1,-0.9]$ and $[0.9,1]$ is presented in Tables 10 for variations in clay, ash, WDF percentages and temperature.

3.2.1. Sensitivity analysis by one-at-a-time (OAT) method

Sensitivity analysis performed based on SPEA values determines the existence of an influence between any input and output variables and the direction of influence. The magnitude of influence requires other sensitivity analysis methods. In this study, OAT method will be employed to assess the importance of input variables in terms of their influence on outputs. OAT methods [35] require defining a reference case in terms of input X and output Y sets and varying one input only x_i. The magnitude and the direction of change in output set is a metric of relative influence of x_i on output set variables $y_j, j = 1 \cdots N_O$ in terms of both direction and magnitude. Let a reference set (measured values):

$$X = \left[x_{ij}\right],\ i = 1..N_1,\ j = 1..N \tag{6}$$

and the corresponding output set:

$$Y = \left[y_{ij}\right],\ i = 1..N_0,\ j = 1..N \tag{7}$$

A variation δ_i applied to x_{ij} will produce a test set, as follows:

$$X_{\delta}^{ij} = \left[x_{1j} \cdots x_{i-1j}\ x_{ij} + \delta_{ij}\ x_{i+1j} \cdots x_{N_1 j}\right] \tag{8}$$

An output set will result after applying X_{δ}^{ij} to the input of the ANN model:

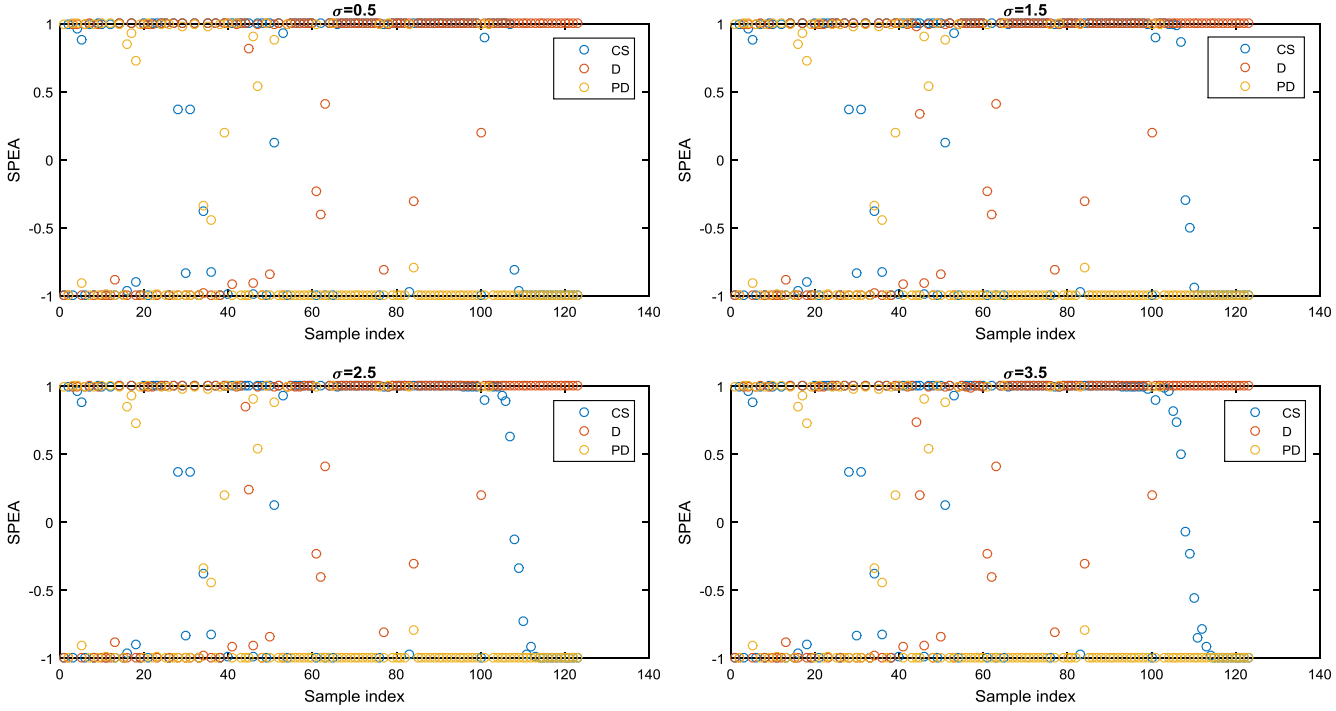

Fig. 9. Spearman rank-order coefficients (clay and ash percentages vary, WDF = const.)

Table 10A
SPEA values greater than 0.9 and lower than −0.9 for variations in Clay % (Ash % varies, WDF %= const.) and output trends triggered by variations in Ash %

	$\sigma_p^{Clay} = 0.5$		$\sigma_p^{Clay} = 1.5$		$\sigma_p^{Clay} = 2.5$		$\sigma_p^{Clay} = 3.5$	
*SPEA*values	> 0.9	< −0.9	> 0.9	< −0.9	> 0.9	< −0.9	> 0.9	< −0.9
Compressive strength↑	75	38	74	37	73	36	72	34
Density↑	90	24	90	24	89	24	89	24
Pore density↓	29	86	29	86	29	86	29	86

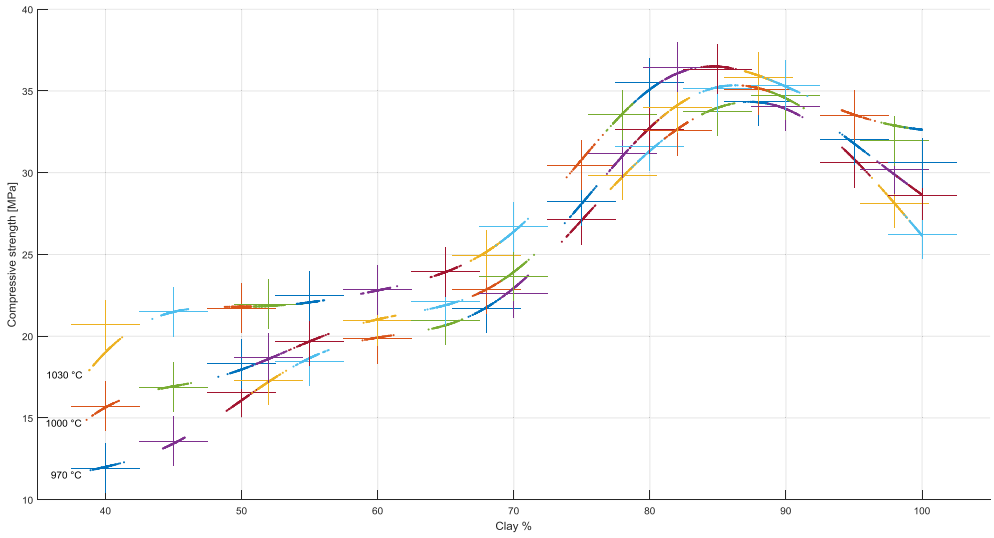

Fig. 10. *CS* – Output of ANN model for Gaussian noise with $\sigma = 0.5$ applied to clay % input and measured values (markers).

Table 10B
SPEA values greater than 0.9 and lower than −0.9 for variations in Ash % (WDF % modified, Clay % = const.) and output trends triggered by variations in Ash %

	$\sigma_p^{Ash} = 0.5$		$\sigma_p^{Ash} = 1.5$		$\sigma_p^{Ash} = 2.5$		$\sigma_p^{Ash} = 3.5$	
*SPEA*values	> 0.9	< 0.9	> 0.9	< 0.9	> 0.9	< 0.9	> 0.9	< 0.9
Compressive strength↓	59	56	53	50	50	46	46	42
Density↓	54	64	43	60	36	56	34	49
Pore density↑	74	44	64	42	58	37	50	28

Table 10C
Number of SPEA values greater than 0.9 and lower than −0.9 for variations in WDF % input variable (Clay % modified, Ash %= const.)

	$\sigma_p^{WDF} = 0.5$		$\sigma_p^{WDF} = 1.5$		$\sigma_p^{WDF} = 2.5$		$\sigma_p^{WDF} = 3.5$	
*SPEA*values	> 0.9	< 0.9	> 0.9	< 0.9	> 0.9	< 0.9	> 0.9	< 0.9
Compressive strength↓	48	73	40	72	34	72	24	72
Density↓	17	103	16	102	13	100	11	98
Pore density↑	68	51	70	49	70	43	68	30

Table 10D
Number of SPEA values greater than 0.9 and lower than −0.9 for variations in Temperature input variable (Clay, Ash and WDF % = const.)

	$\sigma_p^{Temp} = 0.5$		$\sigma_p^{Temp} = 1.5$		$\sigma_p^{Temp} = 2.5$		$\sigma_p^{Temp} = 3.5$		$\sigma_p^{Temp} = 4.5$	
*SPEA*values	> 0.9	< 0.9	> 0.9	< 0.9	> 0.9	< 0.9	> 0.9	< 0.9	> 0.9	< 0.9
Compressive strength↑	72	51	72	50	72	46	71	44	69	35
Density↑	73	50	73	49	73	48	71	45	71	41
Pore density↓	59	64	58	63	54	63	49	63	46	63

$$Y_{\delta}^{ij} = \mathbb{N}\left(X_{\delta}^{ij}\right) \tag{9}$$

The relative influence of x_{ij} on $y_k, k = 1..N_O$ is assessed by the magnitude and sign of the quantity $\frac{\Delta y_k}{\delta_{ij}}$. This metric has to be regarded cautiously though due to varying trends in the data set. Depending on the sample index j, not only the absolute value of $\frac{\Delta y_k}{\delta_{ij}}$ can vary significantly but also the sign. Averaging $\frac{\Delta y_k}{\delta_{ij}}$ over all j values is expected to produce a value that may underestimate/overestimate local effects but will reflect the general data trend and will allow a comparison of various inputs influence. The variation in the input variable was considered $\delta_{ij} = 0.005x_{ij}$. A $N_O \times N_I$ influence factor matrix will result, which is presented in Fig. 11 as a Tornado diagram. The trends observed in the Tornado diagram are consistent with the trends derived from distribution of Spearman coefficients in Tables 10 (negative values are equivalent to a decrease in the output variable caused by an increase of the input variable). However, ranking of inputs cannot be carried out by means of values presented in Fig. 11 since the units are not the same.

OAT sensitivity analysis shows that *WDF* percentage is detrimental to compressive strength while it contributes to the increase of the pore density. Pore density is influenced significantly in the sense of increasing by the ash percentage while compressive strength is influenced in the sense of decreasing. This suggests a strong connection between the organic matter content in ash and the quality of the structure formed through firing. The decrease of the pore density that can be observed at the increase of the temperature can be explained by a higher degree of sintering occurring at approximately 1000 °C and higher. Sintering causes melting of

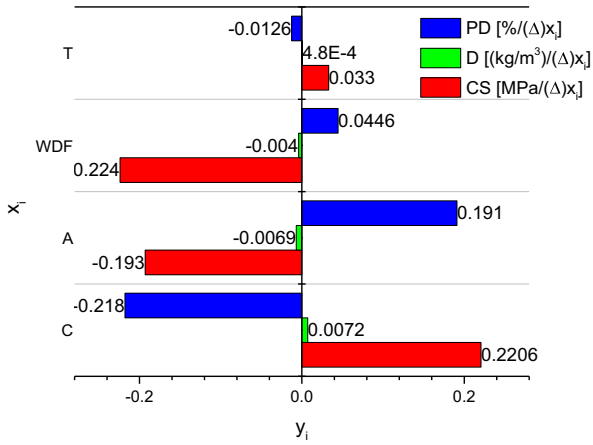

Fig. 11. Influence of input variables (OAT method).

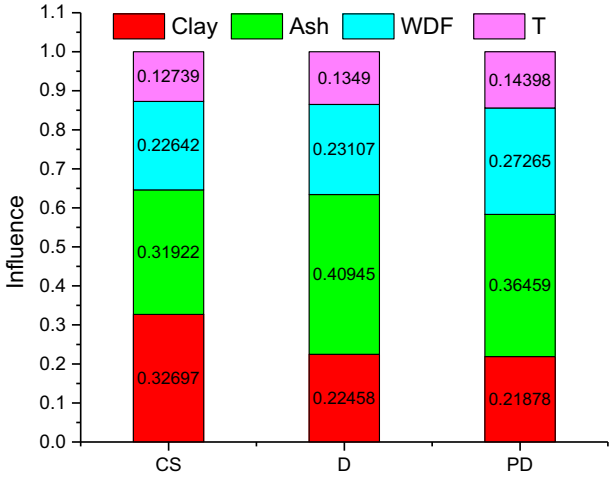

Fig. 12. Individual influence of inputs – Garson algorithm.

the crystalline phases, which flow and fill the internal pore structure due to surface tension forces – Leiva et al [3].

The peak observed in compressive strength (Fig. 10) can be explained by contribution of ash to the formation of the structure, which was observed also by Leiva et al [3]. At the increase of ash percentage the effect of pore formation due to organic matter in ash becomes dominant inhibiting the formation of the structure through sintering. On the other hand, Leiva et al [3] noticed a more pronounced increase of the compressive strength determined by the increase of the ash percentage. The difference was that FA was used in the study with lower value of LOI (1.14) than the one used in this study (Table 1). This can be interpreted as a confirmation of the hypothesis that organic matter contained in ash causes formation of pores in the material structure as a result of combustion during firing, creating faults in the structure. The LOI value (Table 1) quantifies the organic matter content caused by either incomplete combustion, contamination over time in the dump site or both.

The rankings of input variables determined by means of Garson algorithm (Eq. 16) method are presented in Fig. 12.

3.3. Validation of the ANN model

In order to assess how the ANN model is capable of generalizing to an independent data set, cross validation method was employed. Data set DS_2 was fed to the ANN model and a statistical analysis of the output was performed. For data set DS_2 the minimum and maximum values of the components dosage and the variation range for the output variables CS, D and PD are presented in Table 11.

Residuals analysis was performed based on the following criteria:

- zero mean
- independence (no autocorrelation)
- normal distribution
- homoscedasticity

3.3.1. Linear regression analysis

The outputs of the ANN model are presented in Fig. 13 (ANN model predicted vs. measured values) and the main parameters of the linear regression analysis performed on the outputs are presented in Table 12.

On average, the ANN model tends to slightly overestimate (residuals mean values are positive). Mean of residuals are small enough to be considered negligible compared to the corresponding property values. It can be concluded that zero mean of residuals criteria is met.

3.3.2. Independence of residuals

Residuals are plotted against measured values and sample index in Fig. 14. In order to test residuals independence (no autocorrelation), linear regression analysis was performed considering the NN model predicted values as independent variable.

The main results of the linear regression analysis are presented in Table 13.

Analysis of residuals demonstrated that at 95% confidence level the slope of regression line performed between residuals (dependent variable) and predicted values (independent value) is not significantly different from zero. In order to assess quantitatively the residuals independence various statistical tests, such as Durbin-Watson test for autocorrelation can be employed [36]. The null hypothesis H_0 for Durbin-Watson test is that residuals are not autocorrelated. Durbin-Watson test statistic is given by:

$$d = \frac{\sum_{i=2}^{N}(\delta_i - \delta_{i-1})^2}{\sum_{i=1}^{N}\delta_i^2} \tag{10}$$

in which δ_i, $i = 1 \cdots N$ are the residuals and N is the number of observations. Upper and lower critical values d_U and d_L are tabulated in the literature as functions of number of explanatory variables, number of observations and significance level. The following cases can occur depending on the value of the Durbin-Watson test statistic:

• $d < d_L$	reject H_0 – positive autocorrelation
• $d > d_U$	do not reject H_0
• $d_L < d < d_U$	test is inconclusive
• $d > 4 - d_L$	reject H_0 – negative autocorrelation
• $d < 4 - d_U$	do not reject H_0
• $d_L < d < d_U$	test is inconclusive

Upper and lower critical values of the Durbin-Watson statistic for one independent variable, 80 observations and significance level 0.05 are 1.61 and 1.66 respectively. It follows that Durbin-Watson test does not point out any first-order autocorrelation effects in CS, D and PD residuals.

Although widely used in autocorrelation testing, some authors do not consider Durbin-Watson test as a formal way to test auto-

Table 11
Measured values of material properties and components dosage ranges – DS_2.

Clay [%]	Ash [%]	WDF [%]	CS {MPa]	D [kg/m^3]	PD [%]
0...92	0...55	5...90	5.98... 29.44	1.31 ... 1.92	24.86 ... 47.27

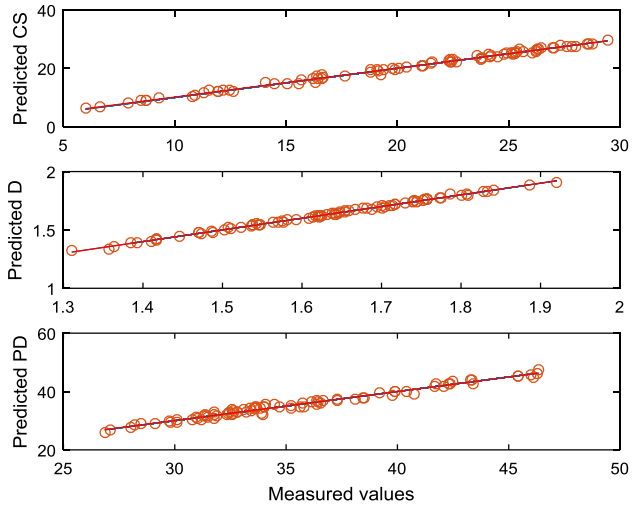

Fig. 13. Outputs of the ANN model for the validation set DS_2.

Table 12
Main parameters of the linear regression model – DS_2.

Parameter	CS	D	PD
Mean of residuals	0.0492	6E−4	0.0177
R^2	0.9965	0.9986	0.9910
Slope	0.9905	1.0031	0.9935
Intercept	0.2407	−0.0045	0.2495
RMSE	0.5091	0.0070	0.6662

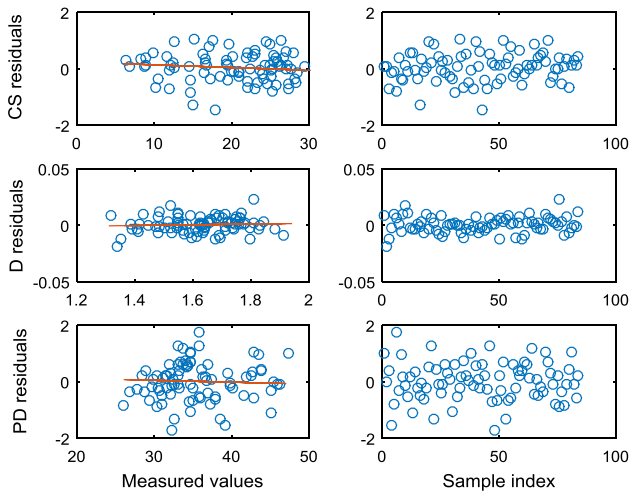

Fig. 14. Residuals plotted against corresponding variable – measured value (left) and against sample index (right).

correlation. One reason is the range of Durbin-Watson statistic in which the test is inconclusive. Further investigation on residuals autocorrelation will be carried out by means of Ljung-Box test for autocorrelation [44]. The null hypothesis for the Ljung-Box test is that residuals are independently distributed (no autocorrelation exists). For the significance level 0.05 the LB statistic

Table 13
Main parameters of the residuals linear regression model – DS_2.

	CS	D	PD
Pearson correlation	−0.1147	0.0589	−0.0.484
Adjusted R Square	0.00112	−0.00867	−0.0098
Intercept	0.240	−0.00449	0.249
Slope	−0.0095	0.00314	−0.00653
Durbin Watson statistic	2.078	1.73	2.070

critical value is listed in Table 14. The rejection of null hypothesis criteria is:

$$LB > LB_{critical} \tag{11}$$

The test results are presented in Table 14 for three values of the lag, 5, 10 and 15. The test fails to reject the null hypothesis for all values of the lag. It can be concluded that residuals of CS, D and PD are independent. Matlab function included in Statistics and Machine Learning Toolbox were used for Ljung-Box tests.

From a practical point of view, it is interesting to analyze the deviation of the ANN model outputs from the measured values. The absolute and relative error histograms for CS, D and PD are represented in Fig. 15. It can be observed that the ANN model is capable of approximating CS and PD within 10% and D within 2%. Maximum relative errors (absolute values) are as follows: CS 8.4%, D 1.5% and PD 5.2%. These observations are in the same range with other results reported in the literature (Table 15).

3.3.3. Normal distribution of residuals

An analytical (formal) and a graphical (less precise but more intuitive) methods will be employed in order to test the normal distribution of residuals. Two standard normal distribution tests, Lilliefors [37] and Anderson-Darling [45] will be employed. Lilliefors test is used to test the null hypothesis that the data sample originates from a normally distributed population when mean and variance of the distribution are not specified.

3.3.3.1. Normal distribution of residuals by Lilliefors test. The characteristic values of the Lilliefors test are presented in Table 16. It can be observed that the test statistic k is smaller than the critical value of the test c, which indicates failure ($h = 0$) to reject the null hypothesis (at 5% significance level) that residuals originate in a normally distributed population.

3.3.3.2. Normal distribution of residuals by Anderson-Darling test. Anderson-Darling test will be performed with the null hypothesis that data originate from a normally distributed population. The same conclusion results from application of Anderson-Darling test (Table 16) that the null hypothesis – data come from a normally distributed population – cannot be rejected at 5% significance level. Matlab functions included in Statistics and Machine Learning Toolbox were used for Lilliefors and Anderson-Darling tests.

3.3.3.3. Graphical inspection of residuals normal distribution. Graphical representation of Q-Q (Quantile-Quantile) plots is commonly employed to assess if a sample comes from a normal distribution (or other distribution). Although not a formal testing of normality of a sample, Q-Q plots can give a good picture of the sample distribution profile.

Table 14
Results of Ljung-Box test for residuals autocorrelation.

	CS			D			PD		
Lag	5	10	15	10	15	10	15	10	15
h	0	0	0	0	0	0	0	0	0
p value	0.376	0.164	0.0618	0.496	0.892	0.944	0.850	0.754	0.822
LB statistic	**5.338**	**14.18**	**24.19**	**0.463**	**4.977**	**7.447**	**1.989**	**6.687**	**9.95**
LB critical value	11.070	18.30	24.99	3.841	18.30	24.99	11.07	18.30	24.99

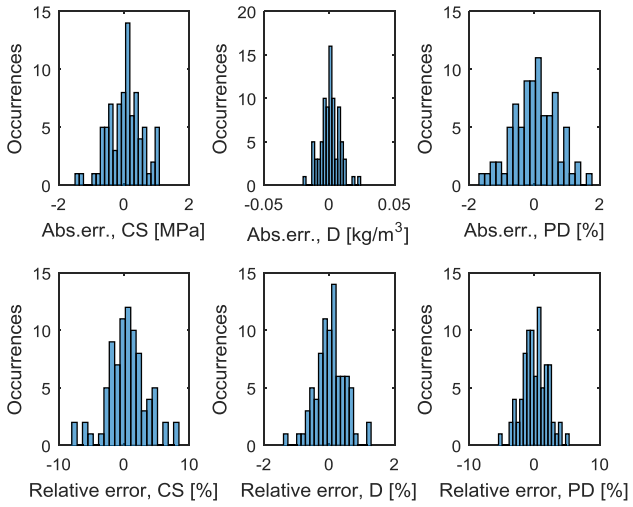

Fig. 15. Histograms of absolute and relative error.

A graphical representation of the Empirical Cumulative Distribution Function (ECDF) for the CS, D and PD residuals is presented in Fig. 16. Normal distribution CDFs to which ECDFs are compared are determined based on mean value and standard deviation of the residuals. Plots of the quantiles (Q-Q plots) of CS, D and PD residuals are presented in Fig. 17. Both ECDF and Q-Q plots suggest a distribution of residuals close to normal.

3.3.4. Homoscedasticity of residuals

A number of statistical tests exist to check the presence of heteroscedasticity in a linear regression model. A standard test for detection of heteroscedasticity is Goldfeld-Quandt test [38]. Goldfeld-Quandt test is performed as follows:

1. NN predicted values are considered explanatory variable while residuals are considered the dependent variable (tested for heteroscedasticity). The sample is sorted in ascending order by values of the explanatory variable.
2. The 84 entries sample is divided in two sub-samples, each containing 32 entries. Sub-sample 1 denoted *SS1* includes entries 1–32 of the data set and sub-sample 2 denoted *SS2* includes entries 53–84. The middle 20 entries are omitted from the analysis.
3. Linear regression analysis is performed on the two sub-samples *SS1* and *SS2*. Let:
   a. $MSE_{max} = \max[MSE(SS1), MSE(SS2)]$ and
   b. $MSE_{min} = \min[MSE(SS1), MSE(SS2)]$

   the largest and the smallest mean squared error respectively.
4. The Goldfeld-Quandt statistic is determined as follows:
   a. $GQ = \frac{MSE_{max}}{MSE_{min}}$
   b. Goldfeld-Quandt statistic tests the equality of error variances using *F* statistic. The critical value of *F* is determined based on the degrees of freedom for each sub-sample for the significance level 0.05 (tabulated in standard statistics textbooks such as [46]):
   c. $F^*_{0.05}(32-1-1, 32-1-1) = F^*_{0.05}(30,30) = 1.84$
5. The criteria to reject the null hypothesis that no heteroscedasticity is present is $GQ > F^*_{0.05}$

The data are presented in Table 17.

From Table 17 it can be observed that the calculated value of *GQ* statistic is smaller than the critical *F* value. It follows that the Goldfeld-Quandt test fails to reject the null hypothesis that no heteroscedasticity is present (significance level 0.05). The Goldfeld-Quandt test confirms homoscedasticity of CS, D and PD residuals.

Table 15
Machine learning models prediction performance – literature review.

Source	Objective, methods	Model prediction performance
Young et al [15]	Statistical and machine learning algorithms to predict the concrete compressive strength based on mixture proportions. Sample size 10,000	Average relative error <10%
Naderpour et al [16]	NN6-18-1 model to simulate concrete compressive strength. Sample size 139	R2 = 0.9/0.89/0.83(Training/Validation/Testing) Max relative error ~ 10%
Deng et al [17]	Convolutional neural network model to predict the compressive strength of concrete. Sample size 50	Average relative error 5.42%, minimum relative error 3.65%
Getahun et al [18]	15-15-2 NN model for concrete compressive strength and tensile splitting strength. Sample size 66	Mean relative error 2.90%, correlation coefficient 0.9811
Alexandridis et al [19]	NN model to predict compressive strength of concrete	Relative error ~ 1%
Šipoš et al [20]	NN model to predict compressive strength of concrete with crushed brick and roof tile aggregate	80% of all predicted data correspond to the relative error equal to or smaller than 10% 100% of the data had a relative error smaller than 17%
Trocoli et al [21]	NN model (17 inputs, 1 output) for compressive strength of concrete. Sample size 1178	Relative error between 20 and 50% for 4.6% of points and larger than 80% in 0.4% of points
Duan et al [22]	14-16-1 NN model to predict compressive strength of recycled aggregate. Sample size 168	Relative error ranging from 0.2% to 16.3% with an average of 5.85%

Table 16
Lilliefors and Anderson-Darling tests results.

Test	CS			D			PD		
	h	Test statistic *k*	Critical value *c*	*h*	Test statistic *k*	Critical value *c*	*h*	Test statistic *k*	Critical value *c*
Lillefors	0	0.054	0.09688	0	0.061	0.09688	0	0.047	0.09688
Anderson Darling	0	0.270	0.7448	0	0.313	0.7448	0	0.143	0.744

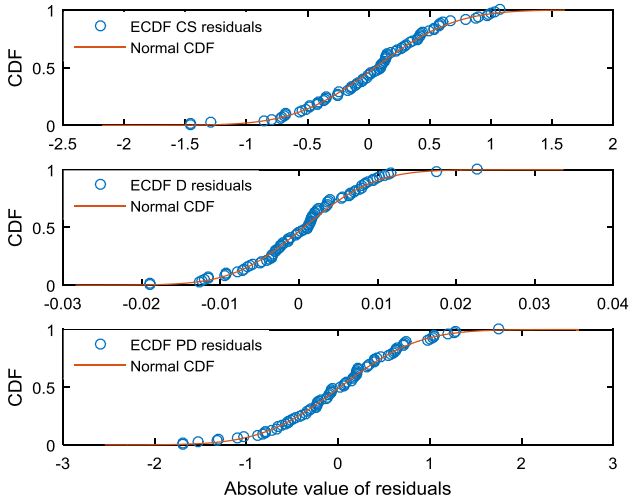

Fig. 16. Empirical Cumulative Distribution Function (ECDF) of residuals compared to the normal CDF.

Further evidence for residuals homoscedasticity can be obtained by applying Engle test [39]. The null hypothesis for Engle test is that residuals are homoscedastic. The test is performed considering significance level 0.05. The null hypothesis can be rejected ($h = 1$) if test statistic is larger than critical value. From Table 17 it can be observed that Engle test fails to reject the null hypothesis, confirming the homoscedasticity of residuals. Matlab function included in Econometrics Toolbox were used for Engle test.

4. Conclusions

Samples of material were manufactured based on clay and two waste materials, ash from coal combustion and waste drilling fluid. The objective of the study was to investigate the extent to which a natural resource – clay can be partially replaced by waste materials, achieving conservation of clay through recycling waste materials existing in site dumps. A key condition of the study was to use the waste materials in a state as close as possible to the raw in order to limit the consumption of energy and resources, thus evaluating to what extent a highly sustainable technology could be developed.

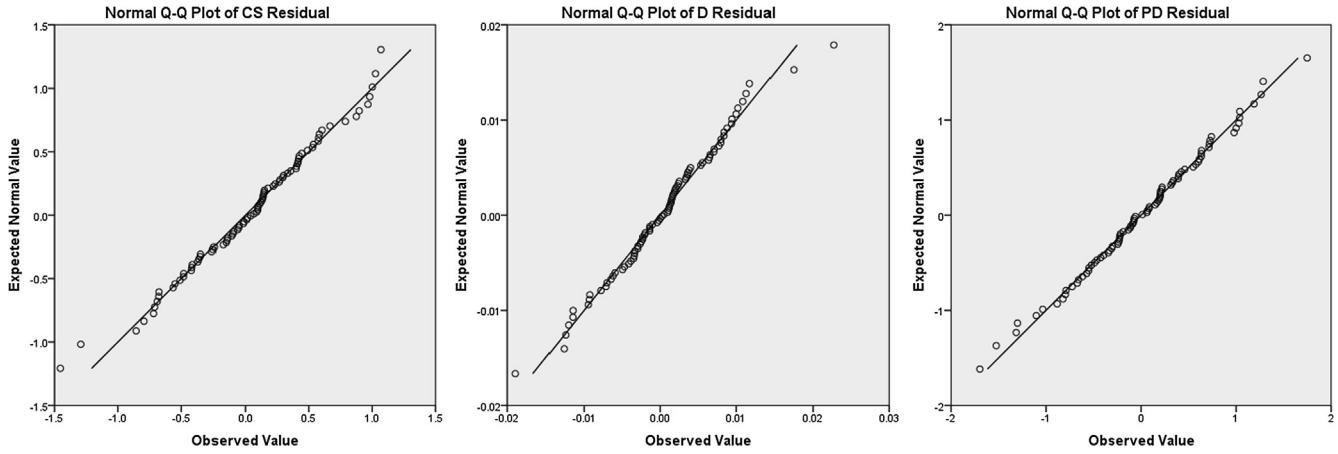

Fig. 17. Q-Q plot of residuals.

Table 17
Goldfeld-Quandt and Engle test results for residuals homoscedasticity.

	*GQ*statistic elements		CS	D	PD
Goldfeld_Quandt test	SS1	*n*	32	32	32
		MSE	0.243	5.77E-5	0.528
	SS2	*n*	32	32	32
		MSE	0.173	5.47E-5	0.384
	*GQ*statistic value		**1.403**	**1.054**	**1.373**
Engle test	*h*		0	0	0
	p value		0.289	0.429	0.965
	Test statistic		1.122	0.624	0.002
	Test statistic critical value		**3.841**	**3.841**	**3.841**

WDF was selected in this study for the following reasons:

- Handling, treatment, neutralizing and disposal are expensive processes
- Few studies regarding recycling WDF for developing construction materials and elements
- Currently, no commercial recycling technology exists for WDF in Romania.

Compressive strength, density and pore density were the properties investigated in this study examining the influence of various parameters (mixture components percentage and firing temperature) on the mechanical properties of the materials. A neural network model was developed to predict compressive strength, apparent density and open pore density depending on the mixture components percentage and firing temperature. The topology of the model was chosen after a series of trials based on performance criteria RMSE and MRE. Validation of the NN model was carried out by means of cross-validation method, using for this purpose an independent data set that was not used in training the model. The performance of the NN model was assessed based on the validation set. Zero mean, normal distribution, absence of autocorrelation and homoscedasticity of residuals were verified. Normal distribution, independence and homoscedasticity of residuals were verified by means of two independent methods.

A sensitivity criterion was introduced assessing the standard deviation of outputs caused by variations of inputs (one at a time) centered at measured values of the input variables with Gaussian distribution and controlled standard deviation values. Sensitivity analysis was performed based on conventional techniques as well, (SPEA and OAT) revealing several data trends. Clay percentage is the component that influences the compressive strength in the sense of increasing, while WDF percentage has the opposite effect. Clay-ash (no WDF) mixture shows an increase of the compressive strength for ash percentage values up to roughly 10% after which the compressive strength drops as ash percentage increases. The initial phase in which the compressive strength increases has been attributed to the influence of ash, which is subject to sintering and contributes to a more solid structure. Further increase of the ash percentage causes a drop of the compressive strength due to the counteracting effect – organic matter present in the ash burns during firing and causes faults of the structure (pores and cracks). The hypothesis is supported by the increase in pore density observed when the ash percentage was increased. Temperature influences positively the compressive strength for any mixture composition. From this point of view, it can be interesting to go beyond the maximum value 1030 °C, which can result in even higher compressive strength values. However, the presence of organic matter in ash will continue to be a limiting factor for compressive strength. Another indication of organic matter transformation/removal during firing is the LOI value for finite products (Table 5) much lower than initial values found in raw materials.

It can be concluded that ash does offer a significant advantage as a substituent for clay only in small percentages if the compressive strength is an acceptance criterion. However, it is expected that ash with lower content of organic matter (such as high grade FA or ash that has been pre-processed to have the organic matter content reduced) can perform better in terms of compressive strength (as it was found in [3]).

Pore density is an interesting property for construction materials if thermal insulation properties of the product are important for a given application. Shimizu et al [43] established a linear relationship between pore density the thermal conductivity. Both WDF and ash contribute similarly to a higher value of the open pore density (as shown in Fig. 11). It follows that thermal conductivity can be modulated (indirectly) by the WDF/ash percentage.

Firing temperature increases the compressive strength and density and reduces the open pore density. It was observed though that increasing the firing temperature values above 1030 °C results in some brittle specimens or specimens with visible cracks and compromised structure. It is hypothesized that the organic matter content in ash causes this effect.

As concluding remarks the following can be formulated:

- Both ash from coal combustion and WDF are compatible with clay and can be used in mixtures with clay to manufacture construction materials. From this point of view, the objective of the study - assess the potential of recyclability of coal ash and WDF was reached.
- Ash and WDF in mixture with clay result in a loss of compressive strength and increase of the open pore density. A reduced value of the compressive strength limits the applicability of the material if load carrying capacity is a selection criterion. Lower density on the other hand reduces the weight of the construction element and higher pore density increases its thermal insulating capacity. From this point of view it can be argued that case-specific optimum solutions can be identified depending on the requirements of the application.
- Specimens manufactured from ash and WDF only have very low values of compressive strength (3–4 MPa). From this point of view it is interesting to consider specimens containing 100% WDF, which have a compressive value (~8 MPa) twice the value of ash – WDF specimens, approximately the same pore density and slightly higher density. However, it was determined that specimens with 100% WDF required a pre-processing phase to reduce humidity (drying at 105 °C for 24 h). Preliminary drying of WDF can be considered as a pre-processing phase that could result in better performance of the finite products. Lower humidity of the WDF can improve its plasticity and as a result its potential to substitute clay.
- It is hypothesized (and confirmed by other studies [3]) that ash with low content of organic matter (such as FA) can significantly improve the compressive strength in mixtures with ash. From this point of view it is interesting to investigate the feasibility of organic matter reduction in the ash already existing in the site dumps. Options include sieving separation and retaining the particle size with lowest organic matter content. Calcination is the most effective method to reduce the organic matter content with the major drawback of significant energy consumption.
- Ash particle size has been proven to influence the properties of the fired specimens [7]. Although this study was designed to use raw waste materials (by raw meaning as little processed as possible) it may be interesting to use lower particle size ash (given the significant difference in particle size distribution between clay and ash) in order to obtain higher values of the compressive strength (which, on the other hand, would limit the ash volume that can be recycled in this way and reduce the technology sustainability). This theory is supported by Bjørk et al [8] where it was found that the sintering behavior (densification rate and final relative density) is inversely proportional to standard deviation and skewness of the PSD function.
- ANNs can be used to predict fairly accurate the properties of construction materials based on recycled coal ash and WDF. In this study, a three-output ANN was used in order to integrate in one model all parameters of interest (compressive strength, apparent density and open porosity). Most studies in the literature consider ANN with one output only: Chithra et al [41], Alexandridis et al [19], Naderpour et al [16], Deng et al [17], Trocoli et al [21], Siddique et al [42], etc. Sensitivity analysis provided insight into the influence of input parameters both

in terms of magnitude and direction of change. It can also be concluded that sensitivity metrics must be regarded cautiously and performing sensitivity analysis through several techniques is recommended.

Declaration of Competing Interest

The authors declare that they have no known competing financial interests or personal relationships that could have appeared to influence the work reported in this paper.

Acknowledgements

This work was funded under 3rd ERA-MIN Joint Call (2015) on Sustainable Supply of Raw Materials in Europe by a grant of Romanian National Authority for Scientific Research and Innovation CCCDI-UEFISCDI, project CHARPHITE Contract no.15/2016.

The author are grateful for the valuable Reviewers' comments, which contributed to gaining further insight into the problem and improved the quality of the paper.

References

[1] Z.T. Yao, X.S. Ji, P.K. Sarker, J.H. Tang, L.Q. Ge, M.S. Xia, Y.Q. Xi, A comprehensive review on the applications of coal fly ash, Earth Sci. Rev. 141 (2015) 105–121.
[2] R.J. Haynes, Reclamation and revegetation of fly ash disposal sites - Challenges and research needs, J. Environ. Manage. 90 (1) (2009 Jan) 43–53.
[3] C. Leiva, C. Arenas, B. Alonso-fariñas, L.F. Vilches, B. Peceño, M. Rodriguez-galán, F. Baena, Characteristics of fired bricks with co-combustion fly ashes, J. Build. Eng. 5 (2016) 114–118.
[4] Xu. Gang, Xianming Shi, Characteristics and applications of fly ash as a sustainable construction material: A state-of-the-art review, Resour. Conserv. Recycl. 136 (2018) 95–109.
[5] M.D.A. Thomas, Optimizing the Use of Fly Ash in Concrete, Portland Cement Association Skokie, IL, 2007.
[6] Safeer Abbas, Muhammad A. Saleem, Syed M.S. Kazmi, Muhammad J. Munir, Production of sustainable clay bricks using waste fly ash: Mechanical and durability properties, J. Build. Eng. 14 (2017) 7–14.
[7] Xu. Lingling, Guo Wei, Wang Tao, Yang Nanru, Study on fired bricks with replacing clay by fly ash in high volume ratio, Constr. Build. Mater. 19 (2005) 243–247.
[8] R. Bjørk, V. Tikare, H.L. Frandsen, N. Pryds, J. Blendell, The effect of particle size distributions on the microstructural evolution during sintering, J. Am. Ceram. Soc. 96 (1) (2013) 103–110.
[9] C. Lirong, H. Min, J. Xuebin, L. Hui, C. Qiang, Z. Min, L. Shenglin, Pilot tests of microbe-soil combined treatment of waste drilling sludge, Nat. Gas Ind. B 2 (2015) 270–276.
[10] X. Zha, X. Liao, X. Zhao, F. Liua, A.Q. He, W.X. Xiong, Turning Waste drilling fluids into a new, sustainable soil resources for landscaping, Ecol. Eng. 121 (2018) 130–136.
[11] Paola Cardoso de Almeida, Ofelia de Queiroz Fernandes Araújo, Jose Luiz de Medeiros, Managing offshore drill cuttings waste for improved sustainability, J. Cleaner Prod. 165 (2017) 143–156.
[12] S.I. Onwukwe, M.S. Nwakaudu, Drilling wastes generation and management approach, Int. J. Environ. Sci. Dev. 3 (3) (2012).
[13] Bamdad Ayati, Chloe Molineux, Darryl Newport, Christopher Cheeseman, Manufacture and performance of lightweight aggregate from waste drill cuttings, J. Cleaner Prod. 208 (2019) 252–260.
[14] Ehsan Mostavi, Somayeh Asadi, Elumeze Ugochukwu, Feasibility study of the potential use of drill cuttings in concrete, Procedia Eng. 118 (2015) 1015–1023.
[15] Benjamin A. Young, Alex Hall, Laurent Pilon, Puneet Gupta, Gaurav Sant, Can the compressive strength of concrete be estimated from knowledge of the mixture proportions?: New insights from statistical analysis and machine learning methods, Cem. Concr. Res. 115 (2019) 379–388, https://doi.org/10.1016/j.cemconres.2018.09.006.
[16] H. Naderpour, A.H. Rafiean, P. Fakharian, Compressive strength prediction of environmentally friendly concrete using artificial neural networks, J. Build. Eng. 16 (2018) 213–219.
[17] Fangming Deng, Yigang He, Shuangxi Zhou, Yu. Yun, Haigen Cheng, Wu. Xiang, Compressive strength prediction of recycled concrete based on deep Learning, Constr. Build. Mater. 175 (2018) 562–569.
[18] M.A. Getahun, S.M. Shitote, C. Zachary, Abiero Gariy, Artificial neural network based modelling approach for strength prediction of concrete incorporating agricultural and construction wastes, Construct. Build. Mater. 190 (2018) 517–525.
[19] Alex Alexandridis, Dimos Triantis, Ilias Stavrakas, Charalampos Stergiopoulos, A neural network approach for compressive strength prediction in cement-based materials through the study of pressure-stimulated electrical signals, Constr. Build. Mater. 30 (2012) 294–300.
[20] Tanja Kalman Šipoš, Ivana Milicevic, Rafat Siddique, Model for mix design of brick aggregate concrete based on neural network modeling, Constr. Build. Mater. 148 (2017) 757–769.
[21] Adriana Trocoli Abdon Dantas, Monica Batista Leite, Koji de Jesus Nagahama, Prediction of compressive strength of concrete containing construction and demolition waste using artificial neural networks, Constr. Build. Mater. 38 (2013) 717–722.
[22] Z.H. Duan, S.C. Kou, C.S. Poon, Prediction of compressive strength of recycled aggregate concrete using artificial neural networks, Constr. Build. Mater. 40 (2013) 1200–1206.
[23] Neural Haykin, Networks and Learning Machines, Pearson, 2008.
[24] Neural Haykin, Networks. A Comprehensive Foundation, Prentice Hall, 1999.
[25] SR EN 993-5 Methods of test for dense shaped refractory products – Part 5: Determination of cold crushing strength.
[26] R. Peck, C. Olsen, J.L. Devore, Introduction to Statistics and Data Analysis, fifth ed., CENAGE Learning, 2016.
[27] SR EN 993-1 Methods of test for dense shaped refractory products – Part 1: Determination of bulk density, apparent porosity and true porosity.
[28] M.T. Hagan, H.B. Demuth, M.H. Beale, O. De Jesús, Neural Network Design, second ed., Martin Hagan, 2002.
[29] Jihao Shi, Yuan Zhu, Faisal Khan, Guoming Chen, Application of Bayesian Regularization Artificial Neural Network in explosion risk analysis of fixed offshore platform, J. Loss Prev. Process Ind. 57 (2019) 131–141.
[30] Yanjun Gan, Qingyun Duan, Wei Gong, Charles Tong, Yunwei Sun, Wei Chu, Aizhong Ye, Chiyuan Miao, Zhenhua Di, A comprehensive evaluation of various sensitivity analysis methods: A case study with a hydrological model, Environ. Modell. Software 51 (2014) 269–285.
[31] Julian D. Olden, Michael K. Joy, Russell G. Death, An accurate comparison of methods for quantifying variable importance in artificial neural networks using simulated data, Ecol. Model. 178 (2004) 389–397.
[32] G.D. Garson, Interpreting neural-network connection weights, Artif. Intell. Expert 6 (1991) 47–51.
[33] Raini Hassan, Wan Haslina Hassan, Imad Fakhri Taha Al-Shaikhli, Salmiah Ahmad, Mojtaba Alizadeh, Feature Ranking Through Weights Manipulations for Artificial Neural Networks-Based Classifiers, 2014 Fifth International Conference on Intelligent Systems, Modelling and Simulation.
[34] Aleksandar I. Jokić, Jovana A. Grahovac, Jelena M. Dodić, Z. Zoltan, Siniša N. Zavargo, Stevan D. Dodić, Popov and Damjan G. Vučurović,, Interpreting the neural network for prediction of fermentation of thick juice from sugar beet processing, APTEFF 42 (2011) 1–288.
[35] E. Borgonovo, E. Plischke, Sensitivity analysis: A review of recent advances, Eur. J. Oper. Res. 248 (2016) 869–887.
[36] D.C. Montgomery, E.A. Peck, G.G. Vining, Introduction to Linear Regression Analysis, third ed., John Wiley & Sons, New York, New York, 2001.
[37] Hubert W. Lilliefors, On the Kolmogorov-Smirnov test for normality with mean and variance unknown, J. Am. Stat. Assoc. 62 (318) (1967).
[38] Stephen M. Goldfeld, R.E. Quandt, Some tests for homoscedasticity, J. Am. Stat. Assoc. 60 (310) (1965) 539–547.
[39] Robert F. Engle, Autoregressive conditional heteroscedasticity with estimates of the variance of United Kingdom Inflation, Econometrica 50 (4) (1982).
[40] Lucica Anghelescu, Possibilities of Recycling Wastes Resulting from Power Industry in Order to Reduce the Environmental Impact PhD thesis, University of Petroşani (Romania), 2015.
[41] S. Chithra, S.R.R. Senthil Kumar, K. Chinnaraju, F., Alfin Ashmita, A comparative study on the compressive strength prediction models for High Performance Concrete containing nano silica and copper slag using regression analysis and Artificial Neural Networks, Constr. Build. Mater. 114 (2016) 528–535.
[42] Rafat Siddique, Paratibha Aggarwal, Yogesh Aggarwal, Prediction of compressive strength of self-compacting concrete containing bottom ash using artificial neural networks, Adv. Eng. Softw. 42 (2011) 780–786.
[43] Toru Shimizu, Kazuhiro Matsuura, Harumi Furue, Kunio Matsuzak, Thermal conductivity of high porosity alumina refractory bricks made by a slurry gelation and foaming method, J. Eur. Ceram. Soc. 33 (2013) 3429–3435.
[44] G.M. Ljung, G.E.P. Box, On a measure of a lack of fit in time series models, Biometrika 65 (2) (1978).
[45] T.W. Anderson, D.A. Darling, A test of goodness-of-fit, J. Am. Stat. Assoc. 49 (1954).
[46] http://socr.ucla.edu/Applets.dir/F_Table.html#FTable0.05.